Uptake of Phenol on Aerosol Particles†

Hanne Falsig,* Allan Gross,‡ Jacob Kongsted,§ Anders Osted,⊥ Marianne Sloth,|| and Kurt V. Mikkelsen#

Department of Chemistry, H. C. Ørsted Institute, University of Copenhagen, Universitetsparken 5, 2100 Copenhagen Ø, Denmark

Ove Christiansen○

Department of Chemistry, University of Aarhus, Langelandsgade 140, 8000 Aarhus C, Denmark

Received: July 1, 2005; In Final Form: November 9, 2005

We present a study of the interaction between a phenol molecule and an aerosol particle. The aerosol particle is represented by a cluster of 128 water molecules. Using a classical approach, we present interaction energy surfaces for different relative distances and for three orientations of phenol relative to the particle. From the energy surfaces we find the reaction pathways with the largest interaction between the molecule and the particle. We use a quantum mechanics/molecular mechanics (QM/MM) method to calculate a potential energy curve for each reaction path. Coupled cluster methods are used for the part of the system described by quantum mechanics, while the part described by molecular mechanics is represented by a polarizable force field. We compare results obtained from the classical approach with the QM/MM results. Furthermore, we use the QM/MM results to calculate mass accommodation coefficients using a quantum-statistical (QM-ST) model and show how the mass accommodation coefficient depends on the relative orientation of phenol with respect to the aerosol particle.

I. Introduction

An aerosol is a system of particles that are uniformly distributed in a uniquely divided state through a gas, usually air. In the atmosphere, aerosol particles form condensation nuclei upon which water vapor condensation begins. Natural and manmade fires over land and wave action over the oceans are the main providers of condensation nuclei. The mixing of hygroscopic material, dust, and soil particles that are blown into the atmosphere also give rise to condensation nuclei. Generally, aerosols serve as initiation sites for the condensation or deposition of water vapor. Atmospheric particles influence the climate directly and indirectly. The direct impact is on the radiation balance since particles absorb and scatter solar and terrestrial radiation.[1] Hydrophilic aerosols can act as cloud condensation nuclei and by this indirectly affect cloud formation processes and cause changes in cloud properties.[1−3] Epidemiological studies show a positive association between exposure to particulate matter and adverse health effects. It has been found that long-term exposure to particulate matter increases the risk of cancer and respiratory diseases, whereas short term effects causes irritation in the bronchitis, asthma and other respiratory diseases.[4−6] Gas-phase molecules in the atmosphere can influence the growth and chemical composition of aerosol particles. The size and composition of aerosol particles is therefore important knowledge that is needed in order to understand the impact on climate and human health.

The main sources of phenol emission into the atmosphere are automobile exhaust, industrial processes, and wood burning. Emissions of phenol have been estimated to be 1900 Tg/year from automobile exhaust and 2300 Tg/year from wood burning.[7] In the industry, phenol is mainly used for manifaction of phenolic resins (45%), bisphenol A (25%), and caprolactam (15%).[8] Measurements show that the concentration of phenol in the ambient environment is considerably higher in urban areas than in more remote locations.[9] Studies in urban areas indicate a concentration of phenol between 1.8 and 13.8 ppbC.[9−11] The formation of phenol in the atmosphere is due to reactions involving alkylbenzenes in both the gas-phase and the liquid-phase. From the reaction between benzene and the hydroxyl radical (OH) phenol is formed in substantial yield. Recent outdoor and indoor chamber studies have found that the product yield of phenol from the benzene + OH reaction is (53.1 ± 6.6)%.[12] Other studies report phenol yields around 25% using various techniques.[13−15]

The degradation of phenol in the gas-phase takes place via the reaction with OH in the daytime and the reaction with the nitrate radical (NO_3) at night.[16] The reaction of OH with phenol in the presence of NO_x has been studied using FT-IR spectroscopy and a large volume reactor by Olariu et al.[17] The major reaction products and their molar yields are 1,2-dihydroxybenzene (80.4 ± 12.1%), 1,4-benzoquinone (3.7 ± 1.2%), and 2-nitrophenol (5.8 ± 1.0%). From the NO_3 initiated oxidation of phenol, 2-nitrophenol and 4-nitrophenol are the most

† Part of the special issue "Donald G. Truhlar Festschrift".

* To whom correspondence should be addressed. E-mail: hanne@theory.ki.ku.dk.
‡ E-mail: agr@dmi.dk.
§ E-mail: kongsted@chem.au.dk.
⊥ E-mail: osted@theory.ki.ku.dk.
|| E-mail: ms@theory.ki.ku.dk.
E-mail: kmi@theory.ki.ku.dk.
○ E-mail: ove@chem.au.dk.

10.1021/jp0536201 CCC: $33.50 © 2006 American Chemical Society
Published on Web 12/03/2005

important products. The formation yields of the products depend on the initial conditions, but they are in the range of 25−50%.[14,18] The residence time of phenol in the atmosphere due to reaction with OH and NO_3 has been estimated by Olariu[16] for daytime and nighttime scenarios. The residence time in the daytime due to the reaction with the hydroxyl radical has been estimated to be 6.4 h. At night, the estimated residence time of phenol due to reaction with NO_3 is 8.1 min. An additional sink for phenol in the atmosphere is the removal by wet and dry deposition. In the condensed phase nitration of phenol results in nitrophenols. Phenol and nitrophenols have been found in clouds, fog, and rain.[9,19−24] Furthermore, phenol and nitrated methylphenols have been found in the secondary organic aerosol from toluene photooxidation.[25] Heal et al. pointed out that the atmospheric lifetime of phenol due to uptake by aerosols is comparable with the lifetime due to the gas-phase oxidation by the hydroxyl radical.[26] Phenol and especially the nitrophenols are of concern to the human health since inhalation is known to cause headache, breathing difficulties, and a rise in body temperature. Concerning 4-nitrophenol, it is known to be cytotoxic and mutagenic and is a suspected carciogenic.[27,28] Furthermore, nitrophenols are thought to be involved in the forest decline experienced in Central Europe and North America.[29]

The mass accommodation coefficient is an important parameter for describing the nucleation and growth of aerosols.[30,31] For example, Pandis et al.[30] showed that a change of the mass accommodation coefficient for sulfuric acid from 0.02 to 0.05 reduces the calculated concentration of cloud condensation nuclei in the marine boundary layer by 45%.

To model mass and heat transfer to and from atmospheric particles, it is important to know what happens to a gas molecule when it encounters an aerosol particle.[32] In previous studies, this has been investigated by use of phenomenological methods, scattering models, or microscopic models.[30,33−40] The phenomenological methods and scattering methods do not include any molecular detail. This indicates that these methods will only be able to differentiate between molecules on the basis of size and shape. In general, microscopic models use quantum mechanics to determine interactions between the molecule and the particle. For this reason, microscopic models typically only include a few molecules to represent the particle. This may not be sufficient for obtaining the bulk properties of the particle.

In this study, we investigate the interaction between a phenol molecule and a water particle. To include molecular detail and a description of the aerosol particle with a substantial amount of molecules, we use a quantum mechanics/molecular mechanics (QM/MM) approach to describe the interaction between a phenol molecule and a water particle. Using a classical approach, we calculate interaction energy surfaces for an area located at the center of the water particle for various distances and various orientations of the phenol molecule relative to the water particle. We estimate the main reaction paths for the relative orientations and use the QM/MM approach to calculate the potential energy curves. Finally, we calculate the mass accommodation coefficients for each reaction path using a quantum-statistical (QM-ST) model.

In section II, we describe the classical approach, the QM/MM method and the theory behind the mass accommodation coefficient. In section III, the computational details are described. In section IV, the classical energy surfaces for three relative orientations of phenol with respect to the water particle are presented. We have used the QM/MM method for each minima and for each orientation to calculate potential energy curves. Finally, we have used the results from the QM/MM calculation to determine the total mass accommodation coefficient for the process. The results are discussed in section IV, and section V provides a summary of the main conclusions.

II. Methods

In this section, we present the theory used to describe the interaction between the phenol molecule and the aerosol particle. In part A, we describe the QM/MM model and the classical interaction model. The QM/MM model divides the system into two subsystems. The phenol molecule is one subsystem described with quantum mechanics, and the water particle is the other subsystem described with molecular mechanics. In part B, we describe the theory of the model applied to achieve the mass accommodation coefficients.

A. Classical and QM/MM Interaction Models. The combined quantum mechanics/molecular mechanics method is based on a partitioning of the total system into several parts treated at different levels of theory. For the system of interest in this work, we consider a partitioning into two parts, where one part is treated using a high level quantum mechanical description (QM) and the rest is treated at the level of molecular mechanics (MM). The Hamiltonian of the total system is correspondingly decomposed into three terms[41−44]

$$\hat{H} = \hat{H}_{QM} + \hat{H}_{QM/MM} + \hat{H}_{MM} \quad (1)$$

where the operator $\hat{H}_{QM}$ is the many-body vacuum Hamiltonian for the QM system, $\hat{H}_{MM}$ describes the classically treated molecules and the operator $\hat{H}_{QM/MM}$ is the interaction Hamiltonian between the two subsystems. The quantum mechanical expectation value of $\hat{H}_{QM}$ and $\hat{H}_{QM/MM}$ yields the QM energy (E_{QM}) and the interaction energy ($E_{QM/MM}$), respectively, while the energy in the MM system is denoted by E_{MM}. The QM/MM energy is further divided into several contributions due to (i) electrostatic interactions, (ii) mutual polarization effects, and (iii) short range and dispersion contributions. In the presented model, the classically treated molecules are represented through point charges (assigned to the nuclei) and molecular dipole polarizabilities assigned to the center-of-mass ($\bar{R}_a$) of each classical molecule. Furthermore, a set of parameters describing the short range and dispersion effects are included for each classical molecule.

In the optimization of the QM/MM electronic wave function, the point charges are introduced into the Hamiltonian for the QM molecule, and the corresponding electrostatic energy is evaluated using quantum mechanics. For the polarization of the classical molecules by the QM system (and vice versa), we use a semiclassical description. Thus, we consider at each center-of-mass of the classical molecules the total electric field ($\mathbf{E}^{tot}(\bar{R}_a)$), which contains contributions from both the QM molecule, the partial charges of the MM molecules, and the field due to the induced dipole moments (μ_a^{ind}) of the MM molecules. These induced dipole moments are in turn related to $\mathbf{E}^{tot}(\bar{R}_a)$, and in a linear approximation, we have

$$\mu_a^{ind} = \alpha \mathbf{E}^{tot}(\vec{R}_a) \quad (2)$$

The term α is the electric dipole polarizability. Since the induced dipole moment at center *a* depends on all the other induced dipole moments in the MM system, an iterative procedure is used for their solution. Having determined the induced dipole moments we define the Hamiltonian accounting for explicit

polarization effects as

$$\hat{H}^{\mathrm{pol}} = -\frac{1}{2}\sum_{a=1}^{A}\mu_a^{\mathrm{ind}}\hat{\mathbf{E}}^{\mathrm{QM}}(\bar{R}_a) \tag{3}$$

where the term $\hat{\mathbf{E}}^{\mathrm{QM}}(\bar{R}_a)$ is the electric field operator at the position of the center of mass of each MM molecule due to the charges (nuclei and electrons) of the QM molecule. The polarization Hamiltonian consists of one-electron contributions and may therefore at relatively low cost be introduced directly into the QM Hamiltonian and thereby directly into the optimization of the wave function.

Dispersion and short-range effects are introduced in an averaged way by including a 6−12 type Lennard-Jones (LJ) potential in the interaction Hamiltonian. We remark that this LJ potential is independent of the electronic coordinates and does therefore not enter the optimization conditions of the wave function.

For the energy in the MM part of the system we consider intramolecular (bonded) and intermolecular (nonbonded) parts. The intermolecular MM/MM energy, $E_{\mathrm{MM/MM}}$, is calculated according to

$$E_{MM/MM} = \frac{1}{2}\sum_{s,s'(s\neq s')}\mathrm{S}\frac{q_s q_{s'}}{|\bar{R}_s - \bar{R}_{s'}|} - \frac{1}{2}\sum_{a=1}^{A}\mu_a^{\mathrm{ind}}E^{s}(\bar{R}_a) + E_{\mathrm{MM/MM}}^{\mathrm{vdw}} \tag{4}$$

where $E_{\mathrm{MM/MM}}^{\mathrm{vdw}}$ is the van der Waals MM/MM energy. Furthermore, the term $\mathbf{E}^{s}(\bar{R}_a)$ is the electric field due to the MM partial charges. We remark that the induced dipole moments depend on the QM wave function and thereby the energy term $E_{\mathrm{MM/MM}}$ implicitly depends on the QM system. In the optimization of the wave function this dependence is included directly.

The QM part of the system is evaluated at the coupled cluster level of theory. This has the advantage that the important dynamical electron−electron correlation is included in the results for the interaction energies. Previous investigations have clearly shown the importance of including the dynamical electron−electron correlation at the coupled cluster level of theory.[45,46] Our focus is an accurate describtion of the quantum mechanical subsystem and that is achieved by a coupled cluster wave function representation of the quantum mechanical subsystem. For theoretical and implementational aspects, as well as previous applications of the combined coupled cluster/molecular mechanics (CC/MM) method, we refer to refs 45−47. The CC/MM method has been implemented at both the coupled cluster singles and doubles (CCSD)[48] and the coupled cluster second-order approximate singles and doubles (CC2)[49,50] levels of theory.[45,46]

The CC2 model is defined upon arguments from perturbation theory. Thus, the QM Hamiltonian is written as $\hat{H} = \hat{F} + \hat{U}$, where $\hat{F}$ is the Fock operator and $\hat{U}$ the fluctuation potential. This partitioning is then introduced into the CCSD optimization equations, and the CC2 model is defined by retaining the singles equations in their original form but keeping only terms in the doubles equations which are correct to first order in the fluctuation potential counting the singles amplitudes as zeroth order parameters. The advantage of the CC2 model as compared to the CCSD description is due to the lower computational scaling. For CCSD this scaling is N^6 whereas the approximations leading to the CC2 model reduces this to an N^5 scaling (N is the number of basis functions). Previously, we have found the CC2/MM method to give accurate results as compared to CCSD/MM for energies and first order properties.[46] Therefore, we will in the following use the computationally less demanding CC2 model.

Also, we explore the energy surfaces related to the interaction between the phenol molecule and the water cluster by a classical approach. The classical analogue of the QM/MM energy is described by

$$E_{\mathrm{cl}} = E_{\mathrm{el,cl}} + E_{\mathrm{pol,cl}} + E_{\mathrm{vdw}} \tag{5}$$

where

$$E_{\mathrm{el,cl}} = \sum_{i,s}\frac{q_i q_s}{|R_i - R_s|} \tag{6}$$

and

$$E_{\mathrm{pol,cl}} = -\frac{1}{2}\sum_{a}P_{\mathrm{ind},a}E^{\mathrm{QM,cl}_a} \tag{7}$$

The subscript, i (s) refers to an atom in the QM (MM) system, $P_{\mathrm{ind},a}$ is the classically evaluated analogue to the induced dipole moment and $E^{\mathrm{QM,cl}_a}$ is the electric field due to phenol. The van der Waals term is given by the corresponding term in the QM/MM method

B. Mass Accommodation Coefficient. A molecule colliding with an aerosol particle can attach to aerosols by physisorption or chemisorption. In physisorption, the molecule is kept on the aerosol by van der Waals and electrostatic interactions. In chemisorption, the molecule sticks to the aerosol by forming a chemical bond. The mass accommodation coefficient is defined as the probability of the molecule to be physisorbed on the particle. The recently developed quantum-statistical (QM-ST) model[51] is used for calculating the mass accommodation coefficient of phenol colliding with a water aerosol particle. The QM-ST model is based on statistical mechanics and phase-space theory and is developed to calculate rate constants for arbitrary bimolecular gas-phase reactions.[52,53] The advantage of the QM-ST model is that rather few parameters are needed for the application of the approach compared to transition state models, molecular reaction dynamics models and reaction path models.[54,55] These include spectroscopic data for the molecule impinging on the aerosol and the potential energy difference between the reaction and product channels.

The classical study of the interactions between phenol and a liquid water aerosol, presented in section IV, shows that the system has six likely reaction paths. To calculate the mass accommodation coefficient, p_{cl}, using the QM-ST model all six reaction paths, denoted $x \in \{1, 2, 3, 4, 5, 6\}$, must be included. The mass accommodation coefficient of the xth product channel, p_{cl}^{x}, can be calculated from

$$\langle p_{\mathrm{cl}}^{x}(E_{\mathrm{tot}}, \bar{v}r^{i}, \bar{v}r^{x})\rangle = \sum_{J=0}^{J_{\max}}(2J+1)\left(\left(\frac{\sum_{\bar{v}r^{x}}N(\bar{v}r^{x}, E_{\mathrm{tot.}}, J)}{\sum_{\bar{v}r^{i}}N(\bar{v}r^{i}, E_{\mathrm{tot.}}, J) + \sum_{x}\sum_{\bar{v}r^{x}}N(\bar{v}r^{x}, E_{\mathrm{tot.}}, J)}\right)\times\left(\sum_{J=0}^{J_{\max}}(2J+1)\right)^{-1}\right) \tag{8}$$

where E_{tot} is the total energy of the system, $\bar{v}r^{x}$ is used to describe the total number of rotational and vibrational quantum

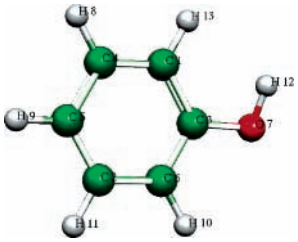

Figure 1. Relative orientation Y_0 of phenol.

numbers of phenol and the particle in channel x, $\bar{v}r^i$ is used to describe the total number of rotational and vibrational quantum numbers for the initial state, J is the total angular momentum number, J_{max} is the maximum total angular momentum number, and $N^x = N(\bar{v}r^x, E_{tot.}, J)$, ($N^i = N(\bar{v}r^i, E_{tot.}, J)$) the phase-space of phenol in channel x, (i). As described in ref 52 less complete distributions can be obtained by assuming a Boltzmann distribution over the initial ro-vibrational states and then summing up over the initial and final ro-vibrational quantum numbers. The total mass accommodation coefficient p_{cl} is calculated as the average of the mass accommodation coefficients for the individual product channels.

III. Computational Details

We use the classical approach and the QM/MM method to investigate the interaction between a phenol molecule and an atmospheric particle. The vacuum structure of phenol is optimized at the MP2/cc-pVTZ[56] level of theory using Gaussian98.[57] Helgaker et al. found that MP2/cc-pVTZ is an attractive compromise between accuracy and cost for calculation of geometries of molecules containing light atoms.[58] The aerosol particle is represented by a cluster containing 128 water molecules. The geometry of the water cluster is obtained from a molecular dynamics simulation. The simulation is performed for a box containing 128 water molecules utilizing periodic boundary conditions together with a spherical cutoff distance of 10.0 Å. The temperature and the pressure are kept constant using 298 K and 0.103 MPa as external values utilizing a scaling procedure. The configuration is obtained as an average of 8000 trajectories starting each from different initial velocities.[59] The simulation time for each trajectory is 20 ps. The water cluster is aligned by placing three oxygen atoms in the xy plane. This plane defines the surface of the water particle. The water cluster used in these calculations was generated to obtain a description of the water molecules in a bulk liquid. However, the properties of the surface may differ for a small cluster and the effect of cluster size is to be investigated. Previously, we have utilized this approach for representing the classical subsystem and observed a very close agreement with the results obtained from a fully dynamical representation.[60,61]

Three orientations of phenol relative to the surface of the water cluster are studied with the classical method. Figures 1−3 show the relative orientations Y_0, Y_1, and Y_2. The distance between the molecule and the surface is for orientation Y_0 defined as the distance between the atom C1 on phenol and the surface of the water particle. For orientation Y_1, the distance is defined as the distance between the C2 atom on phenol and the surface and finally for orientation Y_2, the distance is from the C4 atom and the surface of the water cluster. We calculate the classical interaction energy between phenol and the water cluster. The energy is calculated for many points in an xy plane of an area 6×6 Å^2 situated at the center of the water cluster. This is done for various distances to the water cluster. The resolution in the x-, y-, and z-directions is 0.2 Å. Phenol is

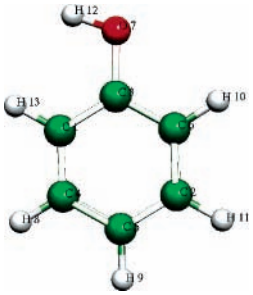

Figure 2. Relative orientation Y_1 of phenol.

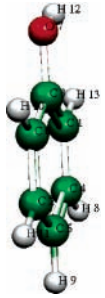

Figure 3. Relative orientation Y_2 of phenol.

TABLE 1: Parameters Used in the Classical and QM/MM Calculations

atom type	A_{ma} (au)	B_{ma} (au)	q (au)
	Water		
O	1.923×10^6	43.17	−0.669
H	0	0	0.3345
	Phenol		
C_1	2.948×10^6	38.49	−0.2605
C_2	2.948×10^6	38.49	−0.0165
C_3	2.948×10^6	38.49	0.3157
C_4	2.948×10^6	38.49	−0.0366
C_5	2.948×10^6	38.49	−0.1596
C_6	2.948×10^6	38.49	−0.1918
O_7	1.575×10^6	41.31	−0.4399
H_8	2.364×10^4	2.124	0.0792
H_9	2.364×10^4	2.124	0.0902
H_{10}	2.364×10^4	2.124	0.1052
H_{11}	2.364×10^4	2.124	0.0715
H_{12}	0	0	0.3036
H_{13}	2.364×10^4	2.124	0.1397

[a] The Lennard-Jones parameters, A_{ma} (attractive) and B_{ma} (repulsive), for water and phenol atoms have been obtained from Jorgensen et al. The atomic charges, q, for water have been obtained from Ahlström et al.[63]

described by the atomic charges and Lennard-Jones parameters given in Table 1. The atomic charges for phenol have been derived using the CHelpG procedure[62] as implemented in Gaussian98 (B3LYP/cc-pVTZ). Furthermore, we constrain the dipole moment to be the ab initio value. The water molecules in the cluster are described by the isotropic polarizability $\alpha = 9.178$ au[63] together with the parameters given in Table 1.

The two most likely reaction paths for each orientation have been obtained from the classical data. We have located the two most attractive points on the energy surfaces for each orientation. We have then chosen a point on the energy surface located farthest away from the aerosol particle. The energy surfaces are located 0.2 Å from each other in the z-direction. We have chosen the most attractive point on the energy surface 0.2 Å closer to the aerosol particle within a radius of 0.4 Å in the xy plane. This procedure has been repeated for all z. We repeated the procedure for a substantial number of starting points at the energy surface farthest from the aerosol particle. For each

TABLE 2: Test of the Basis Set Sensitivity Giving Energies for the Six Minima Employing cc-pVDZ and aug-cc-pVDZ Basis Sets for the Hydrogen Atoms

	energy (kcal/mol)	
reaction path	cc-pVDZ	aug-cc-pVDZ
$Y_{0,1}$	−11.6723	−11.6827
$Y_{0,2}$	−7.8636	−7.8582
$Y_{1,1}$	−5.6487	−5.7792
$Y_{1,2}$	−4.7989	−4.7696
$Y_{2,1}$	−6.1511	−6.1140
$Y_{2,2}$	−4.2067	−4.1724

TABLE 3: Test of the Performance of the CC2/MM Method Compared with CC2 Calculations

orientation	$E_{CC2,BSSE}$ (kcal/mol)	$E_{CC2/MM}$ (kcal/mol)
Y_0	−4.9841	−8.1437
Y_1	−1.7261	−1.7562
Y_2	−1.0280	−0.5932

orientation we have chosen the two reaction paths going through the most attractive points on the energy surfaces. The QM/MM interaction energy has been calculated for each point along each reaction pathway. The QM/MM interaction energy curves for the six most likely reactions paths have been obtained. When using the QM/MM methods, the phenol molecule is the QM system and the water particle is the MM subsystem. A local version of the Dalton program package[64] with the CC/MM code implemented is used to perform the QM/MM calculations at the CC2 level of theory.[50,65] For the QM system the basis set aug-cc-pVDZ[66,67] is applied for carbon and oxygen atoms and cc-pVDZ is applied for the hydrogen atoms. To test the basis set sensitivity we have calculated the energy in the minimum for each of the six most likely reaction paths applying aug-cc-pVDZ for the hydrogen atoms instead of the cc-pVDZ basis set. In Table 2, we compare the energies obtained from using cc-pVDZ and aug-cc-pVDZ on the hydrogen atoms. We find the energy changes at most 2%. Using the basis aug-cc-pVDZ instead of cc-pVDZ for the hydrogen atoms increases the computational cost with 66%. The MM system is described by the same set of parameters as described for the classical approach.

To test the performance of the QM/MM method we have calculated the CC2/MM energy for a system containing phenol and a single water molecule. We have compared the result with the corresponding ab initio result where the system is treated at the CC2 level of theory corrected for the basis-set superposition error (BSSE) by the usual counterpoise correction. For both methods we have employed the aug-cc-pVDZ basis on carbon and oxygen atoms and the cc-pVDZ basis set on the hydrogen atoms as in all the production CC/MM calculations. Three configurations of phenol relative to the water molecule have been considered. The configurations have been obtained based upon the configurations with minimum in energy—one for each of the three relative orientations described above. For each configuration, we have then removed all water molecules except the one closest to the phenol molecule and defined these three phenol−water complexes as test systems. It should be emphasized that the purpose is solely to provide a rough test of the methodology. The MM-parameters used in the CC2/MM calculations have not been optimized for this system, and a larger basis set would certainly be required for highly accurate calculations on these complexes. The results are presented in Table 3. As also discussed in ref 45 the performance of the CC/MM method depends on the type of interaction taking place. In ref 45, it was found in studies on the water dimer that an accurate description of the interface region between the MM part and the QM part can be difficult to obtain, and it was argued that the neglect of exchange-repulsion interactions between the electrons of the QM system and the MM system (as is done in essentially all QM/MM calculations) can be expected to be important in some cases. For the water dimer described as one QM molecule and one MM molecule compared to a full QM description, it was found that if the water molecule described by QM was the proton acceptor rather large errors was obtained. In contrast, in other studies and also for the water dimer with the QM water molecule as the proton donor much smaller deviations were found. In Table 3, very good agreement between the two approaches is found for the Y_1 structure but deviations up to a factor two is found for Y_0 and Y_2, illustrating that also in this study the performance of the QM/MM approach depends on the nature of the configurations and the relative importance of the different interactions. To improve on this situation using QM/MM methods, a considerably more advanced Hamiltonian for the QM/MM interface would need to be developed, accounting for exchange-repulsion as well as including other improvements. Alternatively, some of the nearest water molecules would have to be included in the QM part. This is certainly a promising approach for future work since it gives a full quantum mechanical description within the problematic interface region. However, such calculations would be rather involved for phenol, and this approach has therefore not been pursued in this work.

IV. Results and Discussion

In part A, we present the results obtained from the classical study of the interaction between the phenol molecule and the aerosol particle. In part B, we present the reaction pathways, and finally, in part C, we present the mass accommodation coefficients for the reaction pathways and the total mass accommodation coefficient for the system.

A. The Classical Energy Surfaces. The calculated energy surfaces for the three relative orientations are presented in Figures 4−6. The interaction energy is in kcal/mol. The white areas on the surfaces are the locations where the molecule and the water particle repel each other. The colored areas are the locations where the molecule and the water particle attract each other. In general the interaction energy depends on the approach of the phenol molecule toward the water particle. For orientation Y_0, we find areas on the surface where the molecule is repelled from the surface at all distances. The two most attractive sites at the surface are at $(x, y) = (-3.5, 5.2)$ and at $(x, y) = (0.4, 3.5)$ as shown in Figure 4. The interaction energies at these minima are −6.72 kcal/mol and −3.92 kcal/mol, respectively. For orientation Y_1, at a distance of 4 Å, the interaction energy is negative at all points and hence the phenol molecule is attracted to the surface. In Figure 5 we find the two most attractive sites to be located at $(x, y) = (1.0, 8.0)$ and at $(x, y) = (-3.2, 4.0)$. The energies are −3.59 kcal/mol and −3.01 kcal/mol, respectively. Energy surfaces for orientation Y_2 are presented in Figure 6. As for orientation Y_1 the phenol molecule is attracted to the water cluster at all points for a distance around 4 Å. The two most attractive points are located at $(x, y) = (1.2, 0.4)$ and $(x, y) = (2.8, 2.6)$ with interaction energies of −4.47 kcal/mol and −3.43 kcal/mol, respectively.

It is evident that the interaction energy depends on the location where the molecule approaches and on the orientation of the molecule. We find that the orientation Y_0, where the OH-group on phenol is pointing toward the water surface, is the orientation where the strongest interaction appears.

B. Reaction Pathways. We have calculated the QM/MM interaction energy and the classical energy for each point in

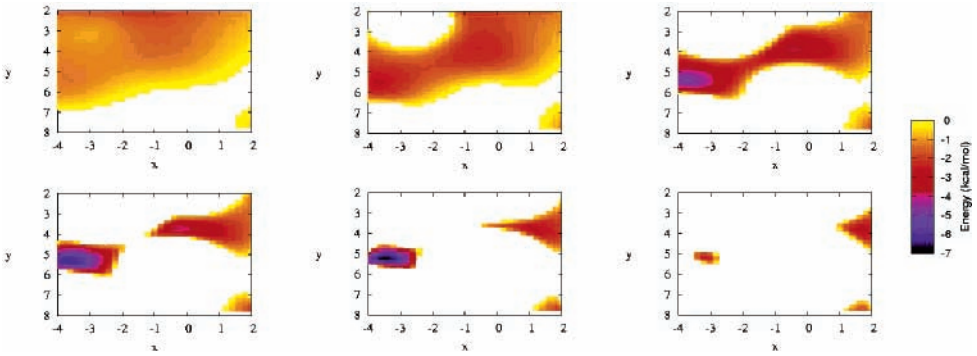

Figure 4. Classical energy surfaces for orientation Y_0. In the first row the distance between the phenol molecule and the surface of the water particle is 5.6, 5.0, and 4.4 Å going from left to right. In the second row 4.0, 3.6, and 3.2 Å going from left to right.

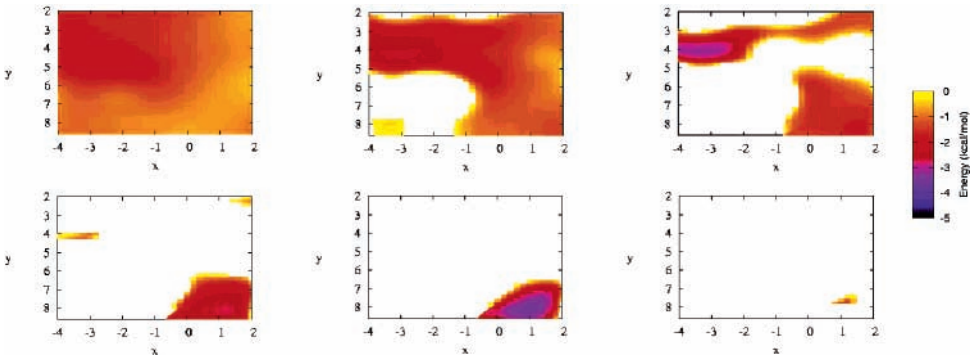

Figure 5. Classical energy surfaces for orientation Y_1. In the first row the distance between the phenol molecule and the surface of the water particle is 4.0, 3.4, and 3.0 Å going from left to right. In the second row 2.4, 2.0, and 1.4 Å going from left to right.

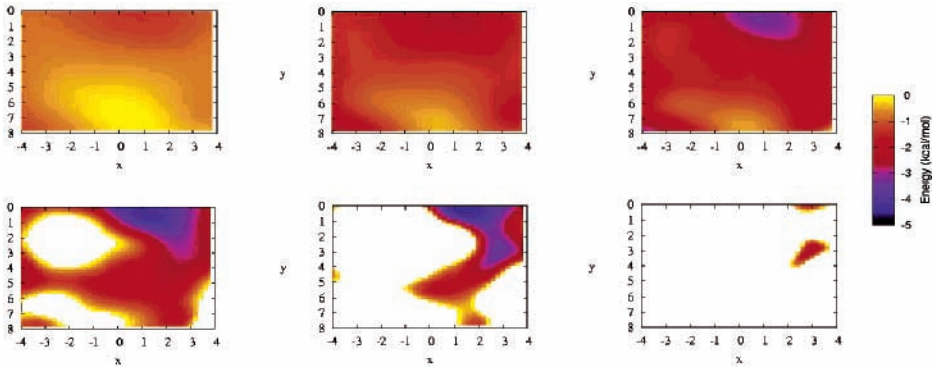

Figure 6. Classical energy surfaces for orientation Y_2. In the first row the distance between the phenol molecule and the surface of the water particle is 5.0, 4.2, and 3.8 Å going from left to right. In the second row 3.4, 3.0, and 2.6 Å going from left to right.

the reaction pathways. The potential energy curves for pathway $Y_{0,1}$, $Y_{0,2}$, $Y_{1,1}$ $Y_{1,2}$, $Y_{2,1}$, and $Y_{2,2}$ are presented in Figure 7a−f for both methods. Here pathway $Y_{n,m}$ is a pathway for orientation Y_n and minima number m. We have used the classical data to obtain the reaction path and then calculated the QM/MM energy for each point in the reaction path, which explains why the QM/MM energy curves are not completely smooth in Figure 7, parts a and f. However, it is evident that the energy minimum is located at approximately the same distance to the surface for the classical and the QM/MM method. Hence the energy surfaces calculated using the classical approach provide the necessary information about the location of the minimum in energy but a somewhat different interaction energy.

In Table 4, the interaction energy at the minima calculated using the classical and the CC/MM approaches are compared and the different energy terms are specified. Comparing the classical and the CC/MM approach we find the difference in the interaction energy to be more significant for orientation Y_0 than for orientation Y_1 and Y_2. For reaction paths $Y_{0,1}$ and $Y_{0,2}$, the energy obtained using the classical approach is 55% of the CC/MM energy. In comparison, the classically obtained interaction energy at the minimum for $Y_{1,1}$ and $Y_{1,2}$ are 65% of the CC/MM energy for both orientations. For reaction paths $Y_{2,1}$ and $Y_{2,2}$, we get 73% and 81%, respectively.

From the CC/MM interaction energies at the minimum presented in Table 4, it is evident that when phenol has orientation Y_0 the absolute interaction energy is highest, 7.9 and 11.7 kcal/mol, while orientations Y_1 and Y_2 have (about the same) interaction energies ranging from 4.2 to 6.1 kcal/mol. The shortest distance between an atom in phenol and an atom in the water particle is around 2 Å for orientation Y_0 and between 2 and 2.5 Å for orientation Y_1 and Y_2. Analyzing the different contributions to the CC/MM interaction energy for orientation Y_0, we see that the electrostatic term accounts for 67% for reaction path $Y_{0,1}$ and 73% for reaction path $Y_{0,2}$. The polarization term accounts for 22% of the CC/MM energy while the van der Waals term contributes with 5−11%. In Figure 8a, the

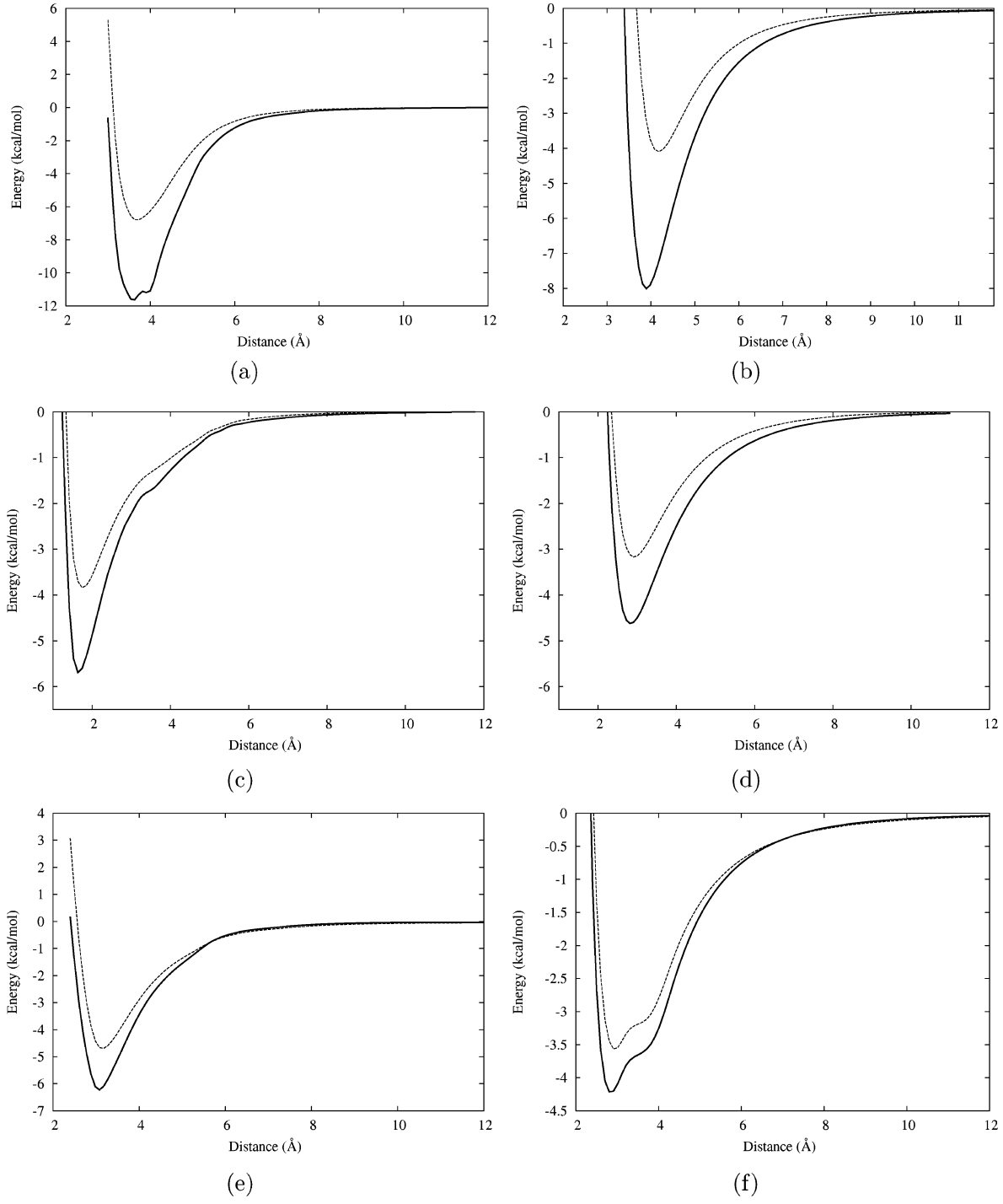

Figure 7. Potential energy curves for reaction path $Y_{0,1}$, $Y_{0,2}$, $Y_{1,1}$, $Y_{1,2}$, $Y_{2,1}$, and $Y_{2,2}$. The dashed lines correspond to energies from the classical calculations. The solid lines correspond to the energies from the QM/MM calculations. Reaction path $Y_{0,1}$ and $Y_{0,2}$ are presented in parts a and b. Reaction path $Y_{1,1}$ and $Y_{1,2}$ are presented in parts c and d. Reaction path $Y_{2,1}$ and $Y_{2,1}$ are presented in parts e and f.

atomic interactions between phenol and the two nearest water molecules are presented for orientation $Y_{0,1}$. It is clear that the main interactions take place between oxygen and hydrogen atoms, with four such interactions within a distance less than 3 Å between the interacting atoms. This explains the dominance of the electrostatic contribution. For reaction path $Y_{1,1}$ and $Y_{1,2}$ the electrostatic term and the van der Waals term contribute equally to the CC/MM interaction energy. The polarization term is of minor importance accounting for 2−5%. In Figure 8b, this is illustrated for orientation $Y_{1,1}$, showing both electrostatic and van der Waals interactions. For orientation Y_2, two rather different situations appear. For reaction path $Y_{2,1}$, the electrostatic term dominates and accounts for 70% of the CC/MM interaction energy, while the van der Waals term contributes with 24%. For reaction path $Y_{2,2}$, the van der Waals term dominates and accounts for 70%, while the electrostatic term contributes with 23%. The difference in the molecular configuration for the two systems are seen in Figure 8, parts c and d. We see that the electrostatic dominance for $Y_{2,1}$ is due to the two interactions between hydrogen and oxygen atoms. The same interaction is observed for orientation $Y_{2,2}$ in Figure 8d, but here the interacting atoms are further apart from each other.

Analyzing the energy terms gives us more detail on the significant difference in the interaction energy for the classical

TABLE 4: Energy Minima from the Classical and CC2/MM Approach for Each Reaction Path and the Different Contributions to the Energy[a]

reaction path	z_{min}	$E_{pol,cl}$	$E_{elec,cl}$	$E_{tot,cl}$	$E_{pol,CC/MM}$	$E_{elec,CC/MM}$	E_{vdw}	$E_{tot,CC/MM}$
$Y_{0,1}$	1.885	−1.2821	−4.2038	−6.7271	−2.5520	−7.8789	−1.3305	−11.6723
$Y_{0,2}$	1.859	−0.8842	−3.959	−3.8108	−1.9208	−6.4122	0.4693	−7.8636
$Y_{1,1}$	2.165	−0.1003	−0.6420	−3.5893	−0.2886	−2.5131	−2.8470	−5.6487
$Y_{1,2}$	2.513	−0.0463	−0.5575	−3.0961	−0.0867	−2.0360	−2.4922	−4.6150
$Y_{2,1}$	2.487	−0.2471	−2.7762	−4.4744	−0.4021	−4.2978	−1.4511	−6.1511
$Y_{2,2}$	2.202	−0.1713	−0.3003	−3.4263	−0.2705	−0.9817	−2.9546	−4.2067

[a] Energies are given in kcal/mol and z_{min} is the shortest distance in (in Å) between one atom on phenol and one atom on a water molecule in the energy minimum.

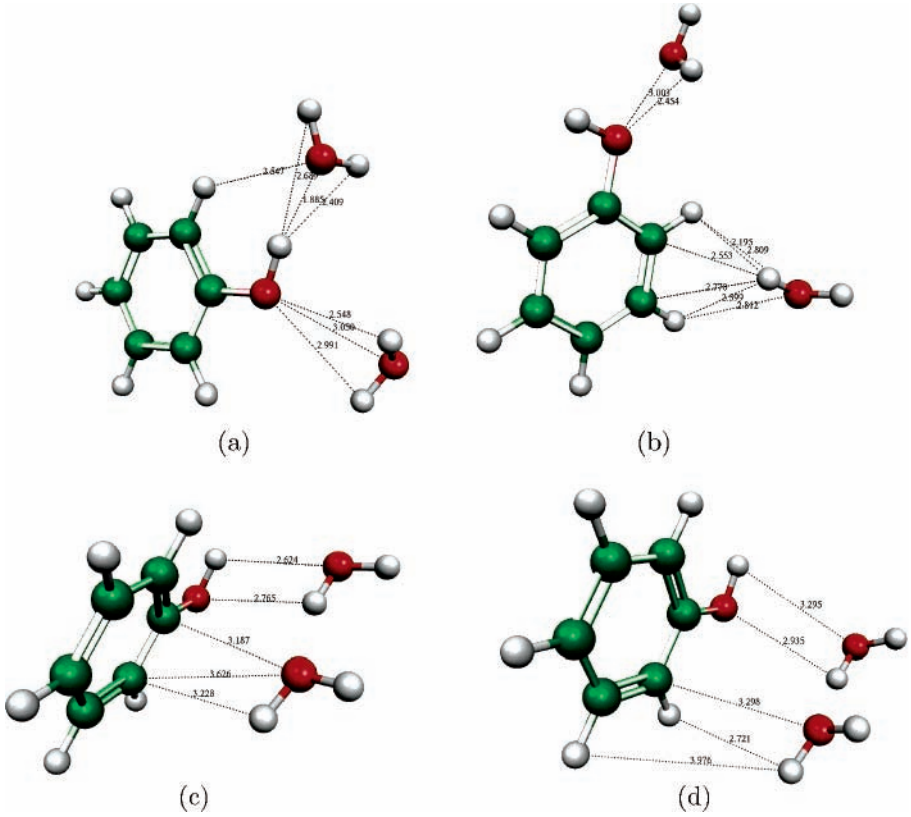

Figure 8. Molecular geometry of phenol and the two water molecules. The water molecules are the two with the shortest distance between the center of mass (COM) of phenol and the COM og water. The geometry in energy minima for reaction path $Y_{0,1}$ is presented in part a. The geometry in energy minima for reaction path $Y_{1,1}$ is presented in part b. The geometry in energy minima for reaction path $Y_{2,1}$ is presented in part c. The geometry in energy minima for reaction path $Y_{2,2}$ is presented in part d.

method and the QM/MM method. In general the polarization term is the minor important contribution. The main difference in interaction energy is due to the electrostatic contribution.

C. Mass Accommodation Coefficient. Figure 9 presents the mass accommodation coefficients as a function of energy and temperature. The figure shows that only reaction paths $Y_{0,1}$, $Y_{1,1}$, and $Y_{2,1}$ have a significant contribution to the total mass accommodation coefficient. At a temperature of 300 K, the reaction paths $Y_{0,1}$, $Y_{1,1}$, and $Y_{2,1}$ contribute approximately 88%, 6%, and 6% to the total mass accommodation coefficient, respectively. The other three channels have negligible influence. The reaction path $Y_{0,1}$ is characterized as the reaction path with the lowest energy minimum among the six reaction paths. The mass accommodation coefficient depends on J_{max} according to eq 8 and J_{max} depends on the long-range potential.[51] We find that $Y_{2,1}$ is the reaction path which has the largest long-range potential contribution. Therefore, the reaction paths $Y_{0,1}$ and $Y_{2,1}$ are the dominant ones. The last figure in Figure 9 shows the total mass accommodation coefficient plotted as a function of temperature. We observe that the total mass accommodation is approximately 0.55 in the entire temperature interval.

To estimate what influence errors in the energies have on the total mass accommodation coefficient, we have calculated the total mass accommodation coefficient using the energy minima of the six reaction paths that are 50% higher or lower. We stress that 50% is a rather abitrary value chosen to investigate the effect. The results are shown together with the total mass accommodation coefficient in the last figure in Figure 9. We observe that 50% variations in the energy minima give variations of less than ±0.1 (about 18%) in the total mass accommodation coefficient in the entire temperature interval from 200 to 300 K.

The temperature dependence of the mass accommodation coefficient calculated in Figure 9 has to our knowledge never been estimated experimentally or theoretically. However, Heal et al.[26] have assumed that $\langle p_{cl}(T) \rangle = 1$ in the analysis of their experiment. They measured the number of phenol molecules entering a liquid water droplet relative to the total number of molecules colliding with the droplet, and they obtained the result $(2.7 \pm 0.5) \times 10^{-2}$ at 283 K.

It is reasonable to assume that after a molecule is physisorbed on the surface it can only desorb or cross the inter-facial and

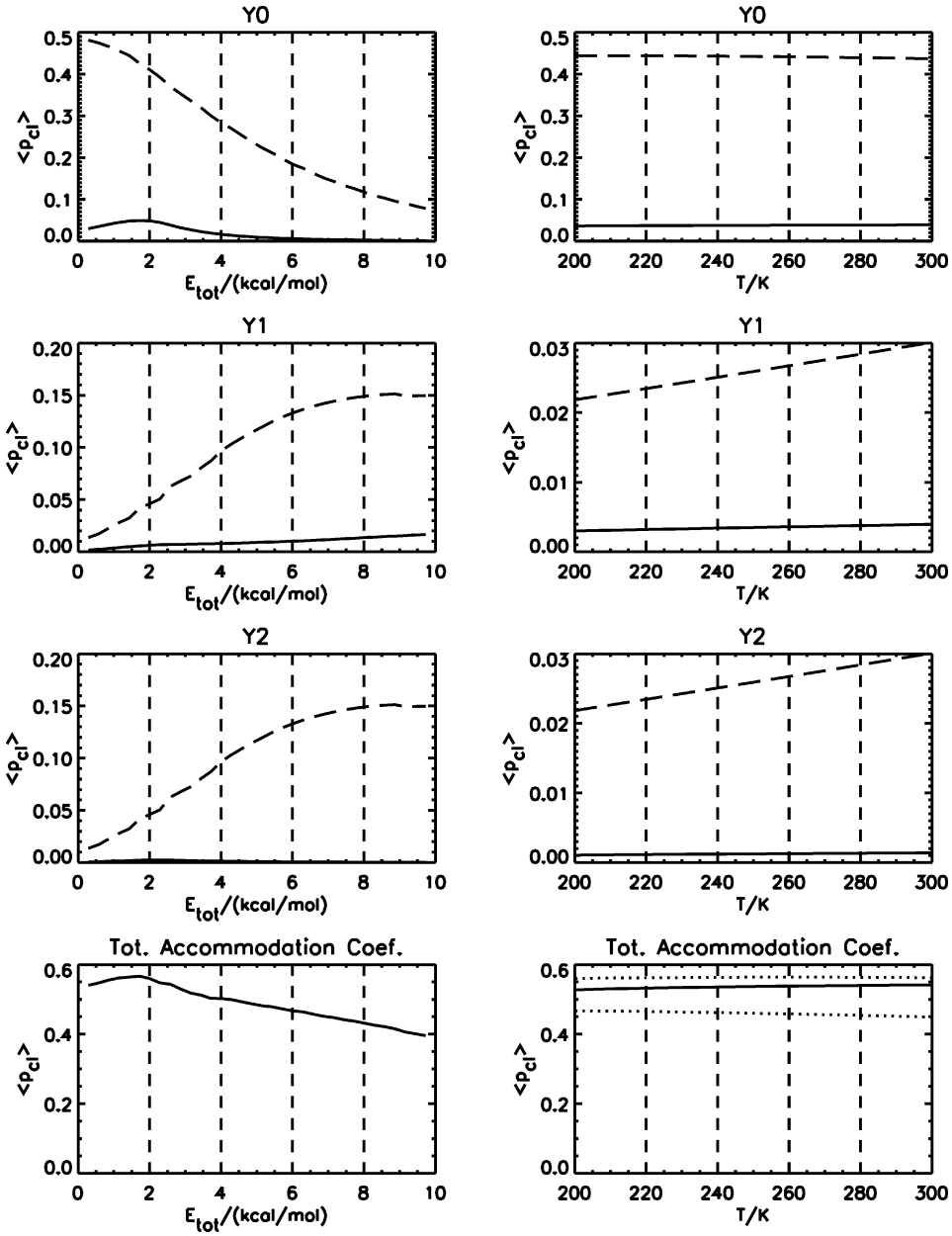

Figure 9. Mass accommodation coefficient as a function of $E_{\text{tot.}}$ and temperature for phenol colliding with a liquid water aerosol. The two upper figures are the mass accommodation coefficients for reaction paths $Y_{0,X}$, in the second row we have figures for reaction paths $Y_{1,X}$, and the figures in the third row is for reaction paths $Y_{2,X}$. The dashed lines correspond to mass accommodation coefficients for reaction paths $Y_{X,1}$ and the solid lines to mass accommodation coefficients for reaction paths $Y_{X,2}$. The lower figures show the total mass accommodation coefficient as a function of energy and temperature. In the last figure the dashed lines represent the total mass accommodation coefficient when the minima have been varied 50%.

enter the aerosol. In Figure 10, we have plotted the total mass accommodation coefficient at a temperature equal to 283 K vs the desorbtion energy, E_{des}, together with the experimentally achieved result. We have assumed that all the weakest bounded molecules desorb from the aerosol, i.e., molecules with binding energies lower than E_{des}. We observe that molecules with binding energies less than $\approx$ 5.0 kcal/mol should desorb in order to achieve agreement with the experimental result.

V. Conclusion

The classical energy surfaces for each orientation show that the interaction energy depends on the orientation of the phenol molecule and on the approach of the phenol molecule toward the particle. Both the classical and QM/MM results show that the strongest interaction takes place when phenol has orientation Y_0. The QM/MM energy calculations give an energy which is

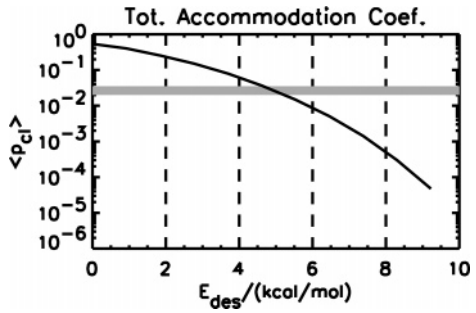

Figure 10. Total mass accommodation coefficient as a function of E_{des} for phenol colliding with a liquid water aerosol at $T = 283$ K. Solid line: result obtain in this work, for further explanation see text. Light gray line: experimental measurement of the number of molecules entering a liquid water droplet relative to the total number of molecules colliding with the droplet at $T = 283$ K.[26]

at least 20% different from the classical results. We conclude that this difference is mainly due to the difference in the description of the electrostatic term.

The calculated mass accommodation coefficients show that phenol will only be adsorbed on the aerosol particle when the molecule collides with the particle at the orientations Y_0 and Y_2. Clearly, this shows that the OH group has a crucial influence on the outcome of this process. This is also seen in Figure 8.

We find a mass accommodation coefficient for phenol impinging on a liquid water aerosol is ≈ 0.55 at temperatures between 200 and 300 K. Though subject to a significant uncertainty this result does not seem to support the general conclusion from Clement et al.[33] that mass accommodation coefficients in general should not be much less than unity.

Acknowledgment. K.V.M. thanks Statens Naturvidenskabelige Forskningsråd, Statens Tekniske Videnskabelige Forskningsråd, the Danish Center for Scientific Computing (DCSC), and the EU-network NANOQUANT for support. A.G. thanks the Danish Center for Scientific Computing for support. O.C. thanks Statens Naturvidenskabelige Forskningsråd, the Danish Center for Scientific Computing (DCSC) and The Danish National Research Foundation for support. M.S. acknowledges a Ph.D. stipend from the Copenhagen Global Change Initiative (COGCI).

References and Notes

(1) Houghton, J. T.; Ding, Y.; Griggs, D. J.; Nogour, M.; van der Linden, P. J.; Dai, X.; Maskell, K.; Johnson, C. A. IPCC 2001.

(2) Novakon, T.; Penner, J. E. *Nature* **1993**, *365*, 823.

(3) Novakov, T.; Corrigan, C. E. *Geophys. Res. Lett.* **1996**, *23*, 2141.

(4) Donaldson, K.; Brown, D.; Clouter, A.; Duffin, R. *J. Aerosol Med.* **2002**, *15*, 213.

(5) Macknee, W.; Donaldson, K. *Eur. Respir. J.* **2003**, *21*, 47.

(6) Li, N.; Sioutas, C.; Schmitz, D.; Misra, C.; Sempf, J.; Wang, M.; Oberley, T.; Froines, J.; Nel, A. *Environ. Health Perspect.* **2003**, *111*, 415.

(7) Lesh, S. A.; Mead, R. C. Prepared by Radian Corporation for U.S. Environmental Protection Agency, Research Triangle Park, N.C.; Contract No. 68-02-3889 1984.

(8) Grosjean, D. *Sci. Total Environ.* **1991**, *100*, 367.

(9) Leuenberger, C.; Ligocki, M. P.; Pankow, J. F. *Environ. Sci. Technol.* **1985**, *19*, 1053.

(10) Kuwata, K.; Uerobi, M.; Yamazaki, Y. *J. Anal. Chem.* **1980**, *52*, 857.

(11) Hoshika, Y.; Muto, G. *J. Chromatogr.* **1978**, *157*, 277.

(12) Volkamer, R.; Klotz, B.; Barnes, I.; Imamura, T.; Wirtz, K.; Washida, N.; Becker, K. H.; Platt, U. *Phys. Chem. Chem. Phys.* **2002**, *4*, 1598.

(13) Bjergbakke, E.; Sillesen, A.; Pagsberg, P. *J. Phys. Chem.* **1996**, *100*, 5729.

(14) Atkinson, R.; Ashmann, S. M.; Arey, J.; Carter, W. P. L. *Chem. Kinet.* **1989**, *21*, 801.

(15) Berndt, T.; Böge, O.; Herrmann, H. *Chem. Phys. Lett.* **1999**, *314*, 435.

(16) Olariu, R. I. Ph.D. Thesis, Faculty of Chemistry, Bergische Universität Gesamthochschule, Wuppertal, Germany, 2001.

(17) Olariu, O. I.; Klotz, B.; Barnes, I.; Becker, K. H.; Mocanu, R. *Atm. Environ.* **2002**, *36*, 3685.

(18) Bolzacchini, E.; Bruschi, M.; Hjorth, J.; Meinardi, S.; Orlandi, M.; Rosenbohm, E. *Environ. Sci. Technol.* **2001**, *35*, 1791.

(19) Lüttke, J.; Levsen, K. *Atm. Environ.* **1997**, *31*, 2649.

(20) Levsen, K.; Behnert, S.; Priess, B.; Svoboda, M.; Winkeler, H. D.; Zietlow, J. *Chemosphere* **1990**, *21*, 1037.

(21) Levsen, K.; Behnert, S.; Mussmann, P.; Raabe, M.; Priess, B. *Int. J. Environ. Anal. Chem.* **1993**, *52*, 87.

(22) Leuenberger, C.; Czuczwa, J.; Tremp, J.; Giger, W. *Chemosphere* **1988**, *17*, 511.

(23) Lüttke, J.; Levsen, K. Acker, K.; Wiesprecht, W.; Möller, D. *Int. J. Environ. Anal. Chem.* **1999**, *74*, 69.

(24) Belloli, R.; Barletta, B.; Bolzacchini, E.; Meinardi, S.; Orlandi, M.; Rindone, B. *J. Chrom. A.* **1999**, *846*, 277.

(25) Forstner, H. J. L.; Flagan, R. C.; Seinfeld, J. H. *Environ. Sci. Technol.* **1997**, *31*, 1345.

(26) Heal, M. R.; Pilling, M. J.; Titcombe, P. E.; Whitaker, B. *J. Geophys. Res. Lett.* **1995**, *22*, 3043.

(27) Fernandez, P.; Grifoll, M.; Solanas, A. M.; Bayona, J. M.; Albaiges, J. *Environ. Sci. Technol.* **1992**, *26*, 817.

(28) Huang, Q.; Wang, L.; Han, S. *Chemosphere* **1995**, *30*, 915.

(29) Rippen, G.; Zietz, E.; Frank, R.; Knacker, T.; Klöpffer, W. *Environ. Technol. Lett.* **1987**, *8*, 475.

(30) Pandis, S. N.; Russel, L. M.; Seinfeld, J. H. *J. Geophys. Res. Atmos.* **1994**, *99*, 16945.

(31) Gross, A.; Baklanov, A. *Int. J. Environ. Pollut.* **2004**, *22* (1/2), 51.

(32) Seinfeld, J. H.; Pandis, S. N. *Atmospheric Chemistry and Physics: From Air Pollution toClimate Change*; John Wiley & Sons: New York, 1998.

(33) Clement, C. F.; Kulmala, M.; Vesala, T. *J. Aerosol Sci.* **1996**, *27*, 869.

(34) Ianni, J. C.; Bandy, A. R. *J. Mol. Struct.* **2000**, *497*, 19.

(35) Bandy, A. R.; Ianni, J. C. *J. Chem. Phys.* **1998**, *A102*, 6533.

(36) Arstilla, H.; Laasonen, K.; Laaksonen, A. *J. Chem. Phys.* **1998**, *108*, 1031.

(37) van Dingenen, R.; Raes, F. *Aerosol Sci. Technol.* **1991**, *15*, 93.

(38) Jayne, J. T.; Duan, S. X.; Davidovits, P.; Worsnop, D. R.; Zahniser, M. S.; Kolb, C. E. *J. Phys. Chem.* **1991**, *95*, 6329.

(39) Davidovits, P.; Jayne, J. T.; Duan, S. X.; Worsnop, D. R.; Zahniser, M. S.; Kolb, C. E. *J. Phys. Chem.* **1991**, *95*, 6337.

(40) Estrin, D. A.; Kohanoff, J.; Laria, D. H.; Weht, R. O. *Chem. Phys. Lett.* **1991**, *280*, 280.

(41) Warshel, A.; Levitt, M. *J. Mol. Biol.* **1976**, *103*, 227.

(42) Singh, U. C.; Kollman, P. A. *J. Comput. Chem.* **1986**, *7*, 718.

(43) Field, M. J.; Bash, P. A.; Karplus, M. *J. Comput. Chem.* **1990**, *11*, 700.

(44) Gao, J.; Xia, X. *Science* **1992**, *258*, 631.

(45) Kongsted, J.; Osted, A.; Mikkelsen, K. V.; Christiansen, O. *J. Phys. Chem. A* **2003**, *107*, 2578.

(46) Osted, A.; Kongsted, J.; Mikkelsen, K. V.; Christiansen, O. *Mol. Phys.* **2003**, *101*, 2055.

(47) Kongsted, J.; Osted, A.; Mikkelsen, K. V.; Christiansen, O. *Mol. Phys.* **2002**, *100*, 1813.

(48) Purvis, G. D.; Bartlett, R. J. *J. Chem. Phys.* **1982**, *76*, 1910.

(49) Christiansen, O.; Koch, H.; Jørgensen, P. J. *Phys. Chem. A* **2003**, *107*, 2578.

(50) Christiansen, O.; Koch, H.; Jørgensen, P. *Chem. Phys. Lett.* **1995**, *243*, 409.

(51) Gross, A.; Mikkelsen, K. V. *Adv. Quantum Chem.*, in press.

(52) Gross, A.; Mikkelsen, K. V.; Stockwell, W. R. *Int. J. Quantum Chem.* **2001**, *84*, 479.

(53) Gross, A.; Mikkelsen, K. V.; Stockwell, W. R. *Int. J. Quantum Chem.* **2001**, *84*, 493.

(54) Billing, G. D.; Mikkelsen, K. V. *Introduction to Molecular Dynamics and Chemichal Kinetics*; John Wiley & Sons: New York, 1996.

(55) Billing, G. D.; Mikkelsen, K. V. *Advanced Molecular Dynamics and Chemichal Kinetics*; JohnWiley & Sons: New York, 1997.

(56) Dunning, T. H. *J. Chem. Phys.* **1989**, *90*, 1007.

(57) Gaussian 98, revision a.11.2 Frisch, M. J.; Trucks, G. W.; Schlegel, H. B.; Scuseria, G. E.; Robb, M. A.; Cheeseman, J. R.; Zakrzewski, V. G.; Montgomery, J. A.; Stratmann, J. R. E.; Burant, J. C.; Dapprich, S.; Millam, J. M.; Daniels, A. D.; Kudin, K. N.; Strain, M. C.; Farkas, O.; Tomasi, J.; Barone, V.; Cossi, M.; Cammi, R.; Mennucci, B.; Pomelli, C.; Adamo, C.; Clifford, S.; Ochterski, J.; Petersson, G. A.; Ayala, P. Y.; Cui, Q.; Morokuma, K.; Rega, N.; Salvador, P.; Dannenberg, J. J.; Malick, D. K.; Rabuck, A. D.; Raghavachari, K.; Foresman, J. B.; Cioslowski, J.; Ortiz, J. V.; Baboul, A. G.; Stefanov, B. B.; Liu, G.; Liashenko, A.; Piskorz, P.; Komaromi, I.; Gomperts, R.; Martin, R. L.; Fox, D. J.; Keith, T.; Al-Laham, M. A.; Peng, C. Y.; Nanayakkara, A.; Challacombe, M.; Gill, P. M. W.; Johnson, B.; Chen, W.; Wong, M. W.; Andres, J. L.; Gonzalez, C.; Head-Gordon, M.; Replogle, E. S.; Pople, J. A. Gaussian, Inc.: Pittsburgh PA, 2001.

(58) Helgaker, T.; Jørgensen, P.; Olsen, J. *Molecular Electronic-Structure Theory*, 1st ed.; John Wiley & Sons: Ltd.: London, 2002.

(59) Billing, G. D.; Mikkelsen, K. V. *Chem. Phys.* **1994**, *182*, 249.

(60) Osted, A.; Kongsted, J.; Mikkelsen, K. V.; Aastrand, P. O.; Christiansen, O. *J. Phys. Chem.* 2005, submitted for publication.

(61) Billing, G. D.; Mikkelsen, K. V. *Chem. Phys.* **1994**, *182*, 249.

(62) Breneman, C. M.; Wiberg, K. B. *J. Comput. Chem.* **1990**, *11*, 361.

(63) Ahlström, P.; Wallquist, A.; Engström, A.; Jönsson, B. *Mol. Phys.* **1989**, *68*, 563.

(64) Dalton, an ab initio electronic structure program, release 1.2, 2001. Helgaker, T.; Jensen, H. J. A.; Jørgensen, P.; Olsen, J.; Ruud, K.; Ågren, H.; Auer, A. A.; Bak, K. L.; Bakken, V.; Christiansen, O.; Coriani, S.; Dahle, P.; Dalskov, E. K.; Enevoldsen, T.; Fernandez, B.; Hättig, C.; Hald, K.; Halkier, A.; Heiberg, H.; Hettema, H.; Jonsson, D.; Kirpekar, S.;

Kobayashi, R.; Koch, H.; Mikkelsen, K. V.; Norman, P.; Packer, M. J.; Pedersen, T. B.; Ruden, T. A.; Sanchez, A.; Saue, T.; Sauer, S. P. A.; Schimmelpfennig, B.; Sylvester-Hvid, K. O.; Taylor, P. R.; Vahtras, O.

(65) Christiansen, O.; Koch, H.; Jørgensen, P.; Helgaker, T. *Chem. Phys. Lett.* **1996**, *263*, 530.

(66) Kendall, R. A.; Dunning, T. H. *J. Chem. Phys.* **1992**, *96*, 6796.

(67) Peterson, K. A.; Kendall, R. A.; Dunning, T. H. *J. Chem. Phys.* **1993**, *99*, 1930.

(68) Jorgensen, W. L.; Maxwell, D. S.; Tirado-Rives, J. *J. Am. Chem. Soc.* **1996**, *118*, 11225.